Received: Added at production | Revised: Added at production | Accepted: Added at production

DOI: xxx/xxxx

RESEARCH ARTICLE

A collision-free pursuit-evasion framework for indirect herding and formation control of non-cooperative UAVs

Ye Zhang | **Yutong Zhu** | **Minghu Tan** | **Jingyu Wang**

[1]School of Astronautics, Northwestern Polytechnical University, Xi'an, China

Correspondence
Corresponding author: Minghu Tan,
Email: mhtan@nwpu.edu.cn

Abstract

In this paper, we aim to design a general framework for the Pursuit-Evasion (PE) game of multiple UAVs. Based on the distance between the pursuers and the evader, the whole pursuit-evasion process is decoupled into a seeking stage and a herding stage. A formation control method is proposed to make sure that the pursuers can find and drive the non-cooperative evaders along a desired trajectory towards the designated target while maintaining a preset formation. In the meantime, an adaptive potential function is designed to achieve collision avoidance to both obstacles and other agents in the formation. The mian contribution is that it combines formation control and collision avoidance in the problem of indirect herding, which is rarely addressed before. Also, the convergence and effectiveness of the designed controller for trajectory tracking and formation maintenance is proved and verified in the paper. Simulation results in two and three dimensional space show that the proposed framework achieves the goal of coordinated herding and collision avoidance in a pursuit-evasion scenario under uncertainties and external disturbances.

KEYWORDS
cooperative control; formation tracking; herding; pursuit-evasion; collision avoidance

1 | INTRODUCTION

In recent years, the applications of unmanned aerial vehicles (UAVs) in the military and civil fields have expanded and demand continues to grow. In these applications, with the increase in mission complexity and reliability requirements, a single UAV is limited by a narrow range of movement, a small operational area and a weak attack capability when performing complicated missions or exploring complex environments[1]. Therefore, the cooperation and coordination of multiple agents play an important role in complex tasks that are difficult for a single agent[2]. To enable these applications, various cooperative capabilities and consensus control methods for multi-agent systems need to be developed[3], including information consensus[4,5], formation control[6,7,8], containmnet control[9] and formation-containment control[10] etc.

Currently, abundant studies have been conducted in the realm of formation control, addressing the problem of consensus control and formation tracking. Considering the intrinsic model uncertainties and disturbances existing in the multi-agent systems, robust control techniques are developed and adopted in formation control. In recent years, some backstepping-based adaptive control methods have been developed for uncertain linear multi-agent systems. In Mahfouz et al.[11], a backstepping PID controller is used to resolve the controversy of formation rearrangement for a troop of cooperative vertical take-off and landing UAVs in a decentralized way that guarantees stability and robustness of the complete formation of the troop. An adaptive fuzzy backstepping controller is proposed by Zhou et al.[12] to solve the formation control problem of under-actuated unmanned surface vehicle in the presence of unknown model nonlinearities and actuator saturation. A novel nonlinear robust close formation controller was developed by Zhang et al.[13], which is based on the command filtered backstepping technique. A new robust finite-time backstepping method is proposed by Yang et al.[14] to solve the practical output tracking problem for a class of nonlinear systems with nonstrict-feedback form. Kartal et al.[15] propose a nonlinear backstepping control method to track desired optimal velocity trajectories for players with generalized Newtonian dynamics.

Apart from such a collaboration mode among multiple agents, there exists another non-cooperative pattern where two opposing groups are considered in the system. For example, the presence of adversarial agents with the aim of causing physical damage to safety-critical infrastructure, can lead to catastrophic consequences. This necessitates protective solutions by either direct physical interception or indirect herding. Such a non-collaborative relationship can be found in a PE game[16], where either evading or pursuing strategies are determined for agents in a predator-prey scenario using the differential game theory[17,18]. Different from traditional pursuit-evasion problems, in indirect herding problems, the influencing or defending agents must pursue non-cooperative roaming agents while also escorting it to a desired location through an inter-agent interaction[19]. The herding method in Pierson et al.[20] utilize a circular-arc formation of herders to influence the nonlinear dynamics of the herd based on a potential-field approach, and designs a point-offset controller to guide the herd close to a specified location. Licitra et al.[21] discuss herding using a switched-system approach, where the herders/pursuers chase evaders/attackers sequentially by switching among them so that certain dwell-time conditions are satisfied to guarantee stability of the resulting trajectories. Deptula et al.[22] use approximate dynamic programming to obtain sub-optimal control policies for the herder to chase a target agent to a goal location. A game-theoretic formulation is used in Nardi et al.[23] to address the herding problem by constructing a virtual barrier, but the computational complexity from the discretization of the state and control-action space limits its applicability. In the above mentioned research, the herders are either in a fixed geometry or move freely in the space, where explicit integration with formation tracking and control of the defenders are rarely discussed.

For practical multi-UAV missions, a large number of UAVs can be tasked in environments riddled with obstacles and wind disturbance. Besides, possible collisions within the formation[24] can affect the movement of each agent. To address the issue of flight safety in critical missions that require high agility in complex and unknown environments, a number of methods have been developed recently, such as model predictive control method[25], which takes the collision-free constraints between the agents as additional relative state constraints in the online optimization problems. Artificial potential fields generate large repelling force when the agents show potential of colliding with obstacles[26]. Another method is based on control barrier functions[27], where the collision-free formation tracking problem with velocity and input-constraints was considered. However, most of the aforementioned approaches to collision or obstacle avoidance have not been widely used in a herding scenario.

Based on the above discussions on related works, it can be summarized that much endeavors have been made in formation control and indirect herding. However, there are still technical challenges remained to be addressed. First, a formation maintenance and tracking problem need to be solved in a herding scenario, where the pursuer need to seek and drive the evaders to the target along a desired trajectory. Second, when pursuing UAVs are in a complex environment and cooperate in a close formation, avoidance of interagent collisions and obstacles need to be considered at the same time to guarantee their flight safety. Besides, most current work only assume a particular form of potential field to model the repulsive motion of the attackers with respect to the defenders. To address the above issues, this paper proposes a novel PE framework to solve the problem of safe formation control of quadrotor UAVs in a complex environment. Compared with previous related works[28,29,30], the main work and contributions of this paper are summarized as follows.

(i) A novel two-staged PE framework is built in this paper, which is decoupled into a seeking stage and a herding stage. A herding formation is proposed to make sure that the pursuers can drive the evaders to the desired target. Compared with previous research, this two-staged framework simplifies the controller design and improves the feasibility of the formation algorithm.

(ii) To solve the problem of non-cooperative formation maintenance in the herding phase, an output-feedback formation maintenance controller based on backstepping is proposed. This controller enables the pursuer to maintain a preset formation while herding the evaders along the desired trajectory. The convergence and effectiveness of the controller is verified in the paper.

(iii) To ensure the safety of the pursuing UAVs during the herding process, a collision avoidance trajectory tracking controller is proposed with the integration of artificial potential functions. We propose to increase the transition area between attractive and repulsive forces by means of a dynamic adjustment factor, allowing both formation aggregation and collision avoidance to be maintained in the formation. Through simulation it is shown that this controller not only achieves the goal of herding formation and collision avoidance at the same time, but also some robustness under uncertainties and external disturbances.

The rest of the paper is organised as follows, Section 2 describes the problems and provides an overview of the PE framework. Section 3 develops a formation maintenance controller for evaders and pursuers and also analyses the controller stability. Section 4 describes the collision avoidance trajectory tracking control law for each UAV, and designs the collision avoidance potential function with the stability analysis of the controller. Simulations are performed in Section 5 to verify the effectiveness of the proposed framework. Finally, conclusions are given in Section 6.

2 | AN OVERVIEW OF THE PURSUIT-EVASION FRAMEWORK

2.1 | Problem description

As illustrated in Fig. 1, the PE problem for two groups of non-cooperative quadrotor UAVs with pursuers and evaders in a Euclidean n-space with some obstacles is considered in this paper. The ultimate goal of the pursuers is to seek and drive the evaders to a desired target along a collision-free trajectory. The whole herding process is divided into two stages: (1) Seeking stage; (2) Herding stage. Recall that the pursuers are required to get closer to the evaders before the pursuers drive the evaders to the target area.

(1) Seeking stage: when the evaders are outside the capture region, the pursuers need to get closer to the evaders and maintaining the pursuing orientation.

(2) Herding stage: the pursuers change their formation in order to drive the evaders to the target area.

In each stage, the pursuers are assumed to circulate information to each other. In other words, as long as one pursuer is in contact with the evader, the other pursuers have access to this information. We use $\mathbf{R}^n$ with some obstacles $\mathbf{O} = \{O_1, O_2, \ldots, O_k, \ldots\}$ represents the Euclidean n-space. $g = [x, y, z]^T \in \mathbf{R}^3$ and $\Theta = [\phi, \theta, \psi]^T \in \mathbf{R}^3$ represent the position vector and attitude vector of the UAV in the inertial system, respectively. The lift in flight of the UAV and its three moments in the direction of attitude angle are provided by the motors on the rotor blades and can be expressed as $\tau = [\tau_1, \tau_2, \tau_3]^T$. $F = [0, 0, T]^T$ denotes the total lift of the UAV. $U = [T, \tau_1, \tau_2, \tau_3]^T$ is denoted as the control input to the UAV and its angular velocity in the inertial system is set to $\omega = [w, q, r]^T$.

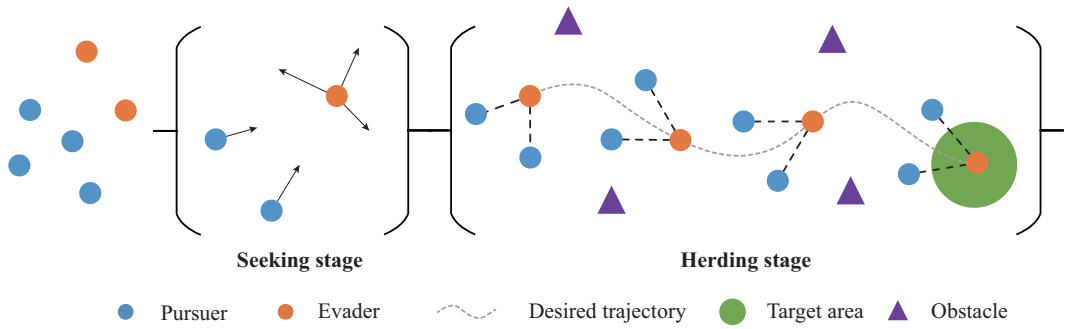

FIGURE 1 Overview of the pursuit-evasion process.

2.2 | Model of the quadcopter UAV

The rotation matrix of the UAV between the inertial and airframe coordinate systems with respect to its angular velocity is

$$\omega = \begin{bmatrix} w \\ q \\ r \end{bmatrix} = \begin{bmatrix} 1 & 0 & -\sin\theta \\ 0 & \cos\phi & \cos\theta\sin\phi \\ 0 & -\sin\phi & \cos\theta\cos\phi \end{bmatrix} \begin{bmatrix} \dot{\phi} \\ \dot{\theta} \\ \dot{\psi} \end{bmatrix} \tag{1}$$

From classical dynamics analysis we can get $m\dot{V} = -mg\xi_1 + u_1 R\xi_1$, where m denotes the mass of the UAV, g is the acceleration of gravity, and $\xi_1 = [0, 0, 1]^T$, u_1 denotes the sum of the lift forces generated by the four motors, that is $u_1 = \sum_{i=1}^{4} F_i = K_t \sum_{i=1}^{4} \Omega_i^2$, where K_t represents the lift coefficient of the UAV, Ω_i denotes the speed of the i-th motor. From the momentum moment theorem, the dynamics equation of the UAV is $J\dot{\omega} = -\omega \times J\omega + \tau$, where J denotes the positive definite inertia matrix of the system, $-\omega \times J\omega$ represents its gyroscopic effect and τ is the control input moment, which is expressed in the form

$$\tau = \begin{bmatrix} \tau_1 \\ \tau_2 \\ \tau_3 \end{bmatrix} = \begin{bmatrix} lK_t(\Omega_2^2 - \Omega_4^2) \\ lK_t(\Omega_1^2 - \Omega_3^2) \\ K_d(\Omega_2^2 + \Omega_4^2 - \Omega_3^2 - \Omega_1^2) \end{bmatrix} \tag{2}$$

where l denotes the distance from the centre of the rotor to the crosshead, K_d denotes the torque factor of the system. The system dynamics model can be divided into a position motion subsystem and an attitude motion subsystem.

$$\begin{bmatrix} \ddot{x} \\ \ddot{y} \\ \ddot{z} \end{bmatrix} = \begin{bmatrix} 0 \\ 0 \\ g \end{bmatrix} - \frac{1}{m} \begin{bmatrix} \cos\phi \sin\theta \cos\psi + \sin\phi \sin\psi \\ \cos\phi \sin\theta \sin\psi - \sin\phi \cos\psi \\ \cos\phi \cos\theta \end{bmatrix} T \tag{3}$$

$$\begin{bmatrix} \dot{w} \\ \dot{q} \\ \dot{r} \end{bmatrix} = \begin{bmatrix} \frac{(J_y - J_z)}{J_x} qr + \frac{J_r}{J_x} \Omega_g q + \frac{1}{J_x} \tau_1 \\ \frac{(J_z - J_x)}{J_y} wr + \frac{J_r}{J_y} \Omega_g w + \frac{1}{J_y} \tau_2 \\ \frac{(J_x - J_y)}{J_z} qw + \frac{1}{J_z} \tau_3 \end{bmatrix} \tag{4}$$

where $\Omega_g = \Omega_1 - \Omega_2 + \Omega_3 - \Omega_4$ and the sum of the rotor inertia of each rotor of the UAV is J_r and J_x, J_y and J_z are the components of the rotational inertia J_r. When the quadrotor is flying at low altitude at a small speed, the angular velocity under the system is approximately equal to the Euler angular velocity, thus

$$\begin{bmatrix} \dot{\phi} \\ \dot{\theta} \\ \dot{\psi} \end{bmatrix} = \begin{bmatrix} w \\ q \\ r \end{bmatrix} \tag{5}$$

Therefore, the formation problem for a group of quadrotor UAVs is studied. In the group, each UAV is modeled by the following dynamics

$$\begin{cases} \ddot{x} = -u_x \dfrac{T}{m} \\ \ddot{y} = -u_y \dfrac{T}{m} \\ \ddot{z} = g - \cos\phi \cos\theta \dfrac{T}{m} \\ \ddot{\phi} = \dot{\theta}\dot{\psi} \left(\dfrac{J_y - J_z}{J_x} \right) + \dfrac{1}{J_x} \tau_1 + \dfrac{J_r}{J_x} \Omega_g \dot{\theta} \\ \ddot{\theta} = \dot{\phi}\dot{\psi} \left(\dfrac{J_z - J_x}{J_y} \right) + \dfrac{1}{J_y} \tau_2 + \dfrac{J_r}{J_y} \Omega_g \dot{\phi} \\ \ddot{\psi} = \dot{\theta}\dot{\phi} \left(\dfrac{J_x - J_y}{J_z} \right) + \dfrac{1}{J_z} \tau_3 \end{cases} \tag{6}$$

where $u_x = \cos\phi \sin\theta \cos\psi + \sin\phi \sin\psi$ and $u_y = \cos\phi \sin\theta \sin\psi - \sin\phi \cos\psi$.

2.3 | The pursuit-evasion framework

According to the problem description, this paper proposes a PE framework illustrated in Fig. 2, which is composed of two stages. At the seeking stage, the pursuers try to approach the evaders in order to enclose them. At the herding stage, the formation control is decoupled into a formation-maintenance problem and a trajectory tracking problem, combining collision-free algorithms, which will be introduced in the following sections.

2.3.1 | At the seeking stage

We set the control input matrix of the UAV system to $U = [T, \tau_1, \tau_2, \tau_3]^T = [U_1, U_2, U_3, U_4]^T$. In practice, the evaders may deviate from their optimal trajectories of the pursuers driving them. This requires the pursuers to approach the evaders in order to enclose them. We use c_p^s, v_p^s and u_p^s and c_e^s, v_e^s and u_e^s to denote the virtual position (formation center), velocity and input acceleration vector of the formation at the seeking stage, where the superscript "s" stands for "seeking" and the subscripts "p" and "e" stand for the "pursuer" and "evader" respectively. Then, during the initial seeking phase the aim of the pursuers is to move as a desired open, rigid formation centered at c_p^s. The formation of the pursuers seeks to: (i) get closer to the evader swarm (i.e., $\|c_p^s(t) - c_e^s(t)\| < E_{trans}^s$, for all $t > T_p^s$, where E_{trans}^s is a user defined parameter, and T_p^s is some finite time at which the seeking phase would be completed), and (ii) maintain the orientation v_p^s of the formation toward the evader swarm (see Fig. 3). We first

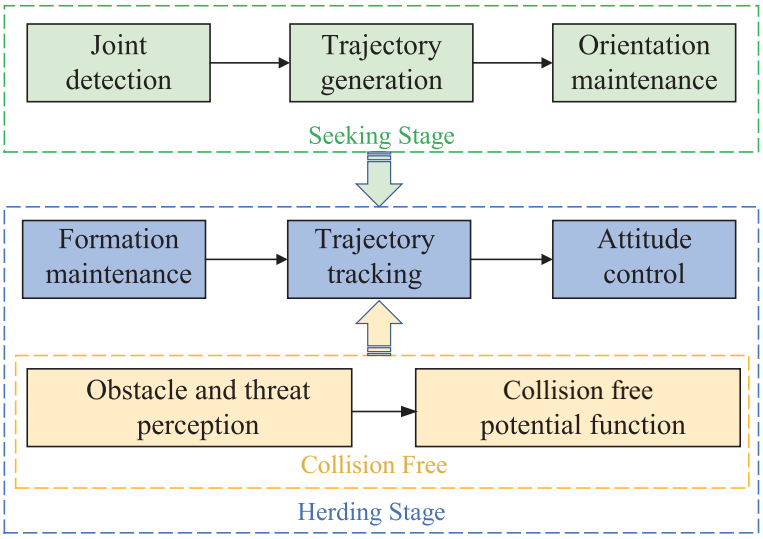

FIGURE 2 A brief illustration of the PE framework.

generate desired trajectories for each pursuer assuming rigid-body motion of the desired formation, and then design finite-time convergent controllers to track the desired trajectories.

In order to generate the desired trajectories that can be tracked by the pursuers, we first consider that the centre c_p^s is controlled by the damped double integrator dynamics, and that the pursuer's motion is governed by:

$$\begin{aligned} \dot{c}_p^s = v_p^s, \quad \dot{v}_p^s = u_p^s - C_D \|v_p^s\| v_p^s \\ \|u_p^s\| \leq \bar{u}_p^s \end{aligned} \tag{7}$$

where $C_D > 0$ is the constant drag coefficient, and the acceleration u_p^s is bounded by $\bar{u}_p^s$ as given in (7). The dynamics in (7) takes into account the air drag experienced by the agents modeled as a quadratic function of the velocity. Note also that the damped double integrator model inherently poses a speed bound on each agent under a limited acceleration control, i.e., $\|v_p^s\| < \bar{v}_p^s = \sqrt{\frac{\bar{u}_p^s}{C_D}}$ and does not require an explicit constraint on the velocity of UAVs while designing bounded controllers, as in earlier literature[31,32]. To design a controller for pursuers in the presence of obstacles, a δ-agent strategy is used[32], where a virtual agent δ is located at the projection point of a pursuer's position on the boundary around the obstacle. The δ-agent moves along the boundary and its velocity is equal to the projection of the pursuer's velocity on the unit tangent vector to the boundary at the current location of the δ-agent. The avoidance control for obstacle O_k is activated only when the δ-agent is within a distance of R_p^o from the formation center using the blending function σ_p^s characterized by R_p^o. Therefore, the control input of the pursuers is designed as:

$$u_p^s = \Omega_{\bar{u}_p^{s_1}} \left[\sum_{k \in I_o} \sigma_p^s u_p^s \mathbf{x}_p^s - \xi_1 \left(c_p^s - c_e^s \right) \right] + \Omega_{\bar{u}_p^{s_2}} \left[C_D \|v_p^s\| v_p^s - \xi_2 \left(v_p^s - v_e^s \right) \right] \tag{8}$$

where $\xi_1, \xi_2 > 0$ are control gains, $\mathbf{x}_p^s = \left[c_p^s, v_p^s, c_\delta^s, v_\delta^s \right]^T$ and c_δ^s, v_δ^s are the position and velocity of the virtual δ-agent on the obstacle O_k corresponding to the pursuers' formation. The summation term in (8) is to avoid collision with obstacles. A saturation function[31,32] $\Omega_{\bar{u}}$: $\mathbf{R}^2 \to \mathbf{R}^2$ is defined as: $\Omega_{\bar{u}}(\mathbf{g}) = \min \left(\|\mathbf{g}\|, \bar{u} \right) \mathbf{g} \|\mathbf{g}\|^{-1}$, where $\bar{u} > 0$ is the saturation limit. To ensure that the desired formation moves with a bounded velocity, i.e., $\|v_p^s\| < \bar{v}_p^s \triangleq \sqrt{\frac{\bar{u}_p^{s_1} + \bar{u}_p^{s_2}}{C_D}}$, two separate saturation functions $\Omega_{\bar{u}_p^{s_1}}, \Omega_{\bar{u}_p^{s_2}}$, with saturation limits $\bar{u}_p^{s_1}$ and $\bar{u}_p^{s_2}$, are used for the terms that correspond to the potentials and velocities, respectively. We add the quadratic term $C_D \|v_p^s\| v_p^s$ to the controller (8) to compensate for the drag term in the dynamics (7).

2.3.2 | At the herding stage

The analysis of the dynamics of the UAV shows that there is no significant coupling between its vertical and horizontal subsystems when simple control is applied to its position. Therefore, when designing the formation at the herding stage, two control methods are used to design the vertical and horizontal position subsystems separately. The vertical position subsystem is

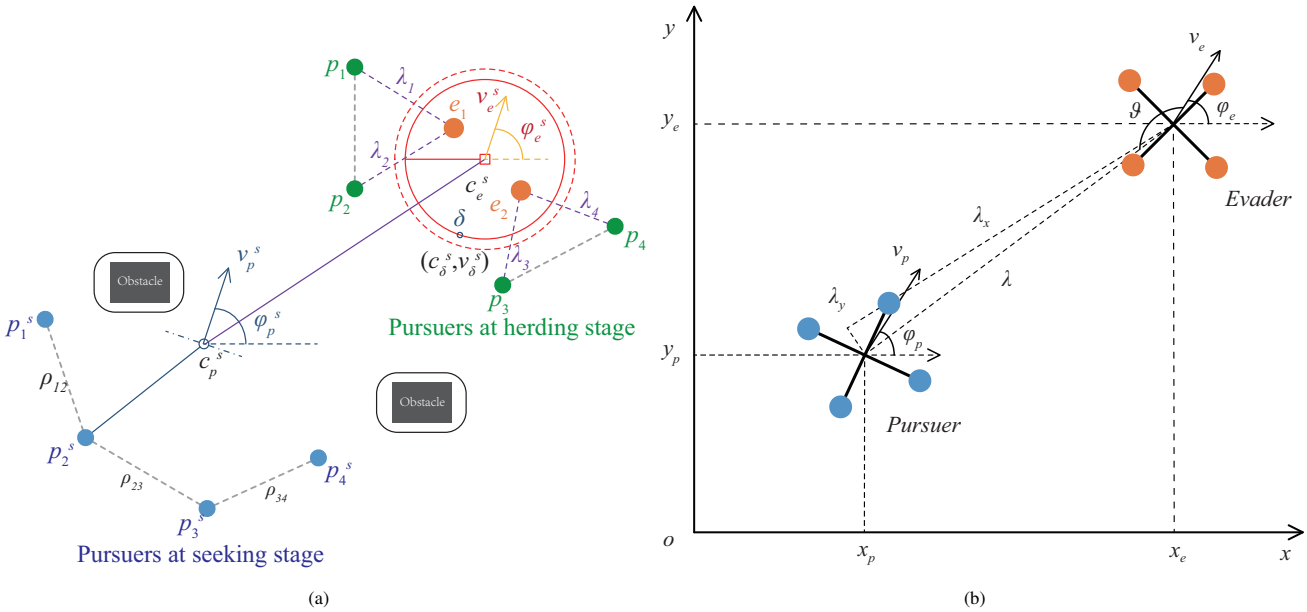

FIGURE 3 (a) Desired positions of the pursuers. (b) Schematic diagram of the formation evader and pursuer structure in the herding phase.

designed as $\dot{z}_p = v_{p_z}$, $\dot{z}_e = v_{e_z}$. As shown in Fig. 3(a), the herding stage is entered after the completion of the seeking phase. At the same altitude, the relative position of the pursuer and evader is shown in Fig. 3(b). A coordinate system is defined for the two-dimensional space. The relative distance to the centre of the UAV is λ, and the velocity of the evader and the pursuer are angled with the x-axis as φ_e and φ_p, respectively. the angle between the line of the centre of the UAV and the direction of the evader's velocity is ϑ.

The horizontal position subsystem of the UAV is

$$\begin{cases} \dot{x} = v\cos\varphi \\ \dot{y} = v\sin\varphi \\ \dot{\varphi} = \omega \end{cases} \tag{9}$$

To make it easier to describe the relative position of the evader and pursuer in the herding stage in the same plane, λ is decomposed along the x-axis and y-axis of the coordinate system into λ_x, λ_y, thus $\lambda_x = -(x_e - x_p)\cos\varphi_e - (y_e - y_p)\sin\varphi_e$ and $\lambda_y = (x_e - x_p)\sin\varphi_e - (y_e - y_p)\cos\varphi_e$. Furthermore, in order to ensure that the formations in the herding phase can always move in the same direction, it is necessary to ensure that $\varphi_p \to \varphi_e$. Therefore, a subsystem for three directions of the formation during flight can be derived. The formation maintenance problem for pursuers in 3D space can be described as

$$\begin{cases} \lim\limits_{t\to\infty}\left(\lambda_x^d - \lambda_x\right) = 0 \\ \lim\limits_{t\to\infty}\left(\lambda_y^d - \lambda_y\right) = 0 \\ \lim\limits_{t\to\infty}\left(\lambda_z^d - \lambda_z\right) = 0 \\ \lim\limits_{t\to\infty}\left(\varphi_p - \varphi_e\right) = 0 \end{cases} \tag{10}$$

where λ_x^d, λ_y^d, λ_z^d denote the desired distance in each of the three axes. $\lambda_z = z_p - z_e$ and we can get

$$\dot{\lambda}_x = \lambda_y\omega_e + \dot{x}_p\cos\varphi_e + \dot{y}_e\sin\varphi_e - (\dot{x}_e\cos\varphi_e + \dot{y}_e\sin\varphi_e) \tag{11}$$

We set the heading angle error to be $e_\varphi = \varphi_p - \varphi_e$ and set v_p, ω_p to be the forward flight velocity and heading angle velocity of the pursuer in the x-o-y plane. A certain velocity constraint exists in the direction perpendicular to the forward flight velocity as

$\dot{y}_p \cos\varphi_p - \dot{x}_p \sin\varphi_p = 0$. By simplifying it through the trigonometric identity we can get

$$\begin{cases} \dot{\lambda}_x = \lambda_y \omega_e + v_p \cos e_\varphi - v_e \\ \dot{\lambda}_y = -\lambda_x \omega_e + v_p \sin e_\varphi \end{cases} \tag{12}$$

where $v_e = \dot{x}_e \cos\varphi_e + \dot{y}_e \sin\varphi_e$. We set λ^d to be the desired relative distance to the centre of the UAV. Thereby the relative position relationship between evader and pursuer can be determined by λ and ϑ, where $\vartheta \in [-\pi, \pi)$ is shown in Fig. 3. Therefore, we can get $\lambda_x^d = \lambda^d \cos\vartheta$ and $\lambda_y^d = \lambda^d \sin\vartheta$. In this case, the formation maintenance problem for pursuers is simplified to $\lambda \to \lambda^d$ and $\vartheta \to \vartheta^d$, which is further converted to $\lambda_x \to \lambda_x^d$ and $\lambda_y \to \lambda_y^d$. When the formation is stable, the relative distance between evader and pursuer λ^d is a preset fixed value, thus $\|\lambda^d\|_2 = \lambda_0$ and $\dot{\lambda}_d = 0$. We get $\dot{\lambda}_x^d = -\lambda_0 \dot{\vartheta} \sin\vartheta$ and $\dot{\lambda}_y^d = \lambda_0 \dot{\vartheta} \cos\vartheta$. The relative position error between evaders and pursuers in the herding phase in the *x*-*o*-*y* plane can be expressed as $e_x = \lambda_x^d - \lambda_x$ and $e_y = \lambda_y^d - \lambda_y$. The relative dynamics of the formation in the herding phase when the formation is in three dimensions can then be represented as

$$\begin{cases} \dot{e}_x = e_y \omega_e - v_p \cos e_\varphi + f_1 \\ \dot{e}_y = -e_x \omega_e - v_p \sin e_\varphi + f_2 \\ \dot{e}_\varphi = \omega_p - \omega_e \\ \dot{e}_z = v_{p_z} - v_{e_z} \end{cases} \tag{13}$$

where we set $f_1 = -\lambda_0 \dot{\vartheta} \sin\vartheta - \lambda_0 \omega_e \sin\vartheta + v_e$ and $f_2 = \lambda_0 \dot{\vartheta} \cos\vartheta + \lambda_0 \omega_e \cos\vartheta$.

Any one of the UAVs in the formation needs to be able to track a predetermined desired trajectory steadily during the flight. In this case, the pursuers drive the evaders' movements and maintain the basic stability of the formation according to the preset formation structure. Therefore, with the formation set in advance, the flight control problem of the formation as a whole is simplified to the flight control problem of the evaders.

For the pursuer, its final trajectory route depends on the size of λ^d. When the formation is moving in a triangular formation, the pursuer needs to satisfy the following conditions

$$\begin{cases} x_p^d = x_e + \lambda_x \cos\varphi_e - \lambda_y \sin\varphi_e \\ y_p^d = y_e + \lambda_x \sin\varphi_e - \lambda_y \cos\varphi_e \\ z_p^d = z_e + \lambda_z \end{cases} \tag{14}$$

Eq.(13) gives the speed required by the pursuer to maintain the formation. Therefore, its trajectory tracking needs to satisfy

$$\begin{cases} \lim\limits_{t\to\infty} \left(v_{p_x}^d - v_{p_x}\right) = 0 \\ \lim\limits_{t\to\infty} \left(v_{p_y}^d - v_{p_y}\right) = 0 \\ \lim\limits_{t\to\infty} \left(v_{p_z}^d - v_{p_z}\right) = 0 \end{cases} \tag{15}$$

where v_p^d is the expected velocity in the pursuer's inertial system, respectively, which is decomposed as $v_{p_x}^d = v_p^d \cos\varphi_p$ and $v_{p_y}^d = v_p^d \sin\varphi_p$. From Fig. 3 it can be seen that the relationship between the pursuer's heading angle and yaw angle in order to maintain the formation is $\psi_p^d = \varphi_p^d - \arctan\left(\frac{v_{p_{yb}}}{v_{p_{xb}}}\right)$, where $v_{p_{xb}}$ and $v_{p_{yb}}$ are the speed from the aircraft coordinate system along the *x*-axis and *y*-axis, respectively.

2.4 | Preliminaries

To obtain the main results of this paper, the following Definitions and Lemmas are provided in this subsection.

Definition 1. Continuous-time non-linear autonomous system is designed to

$$\dot{x} = f(x,t),\ x(t_0) = x_0 \tag{16}$$

where $x \in \mathbf{R}^n$ is an *n*-dimensional state vector and $f : \mathbf{R}^n \to \mathbf{R}^n$ is an *n*-dimensional vector function. If there exists some state quantity x_ε such that $\dot{x}_\varepsilon = f(x_\varepsilon, t) = 0,\ \forall t \geq t_0$. Then, it is called an Equilibrium point or equilibrium state of the system x_ε.

Definition 2. When $e_\varphi \to 0$, we define

$$\Theta = \left\{ x_i(t) \left| x_i(t) \to 0, \forall x_i(0) \in \Theta, t \to \infty \right. \right\} \tag{17}$$

as a bounded closed compact set and take the neighbourhood Γ along the boundary of Θ.

Lemma 1. [33,34] *For Eq. (16), we construct a scalar function $V(x,t)$ with continuous first-order partial derivatives for both x and t, where $V(0,t) = 0$. For all non-zero state points x in the state space that satisfy*

(1) *$V(x,t)$ is positive definite and bounded, namely, there exist two continuous non-decreasing scalar functions $\alpha\|x\|$ and $\beta\|x\|$ in space with $\alpha(0) = 0$ and $\beta(0) = 0$ such that for all $t = [t_0, \infty)$ and all $x \neq 0$ they make*

$$\beta\|x\| \geq V(x,t) \geq \alpha\left(\|x\|\right) > 0 \tag{18}$$

(2) *The derivative $\dot{V}(x,t)$ of $V(x,t)$ with respect to time t is negative definite and bounded, that is there exists a continuous non-decreasing scalar function $\gamma\|x\|$ in space, where $\gamma(0) = 0$, such that for all $t = [t_0, \infty)$ and all $x \neq 0$ they make*

$$\dot{V}(x,t) \leq -\gamma\left(\|x\|\right) < 0 \tag{19}$$

Therefore, the system is asymptotically stable. If it can also be satisfied that when $\|x\| \to \infty$, there is $\alpha\left(\|x\|\right) \to \infty$, namely $V(x,t) \to \infty$. Hence, the equilibrium state $x = 0$ of the system at the origin is globally uniformly asymptotically stable.

Lemma 2. [34,35] *Let Θ be a bounded closed compact set with the property that every solution of (16) which begins in Θ remains for all $t \geq t_0$. Assume there is a scalar function $V(x)$ which has continuous first partials in Θ and is such that $\dot{V}(x) \leq 0$. Let $\mathcal{M}$ be the largest invariant set and every solution starting in Θ approaches $\mathcal{M}$ as $t \to \infty$.*

Lemma 3. [34,35] *Let $V(x)$ be a scalar function with continuous first partials satisfying*

$$\begin{aligned} &V(x) > 0 \quad \textit{for all} \quad x \neq 0 \\ &\dot{V}(x) \leq 0 \quad \textit{for all} \quad x \\ &V(x) \to \infty \quad \textit{as} \quad \|x\| \to \infty \end{aligned} \tag{20}$$

then the system (16) is completely stable.

3 | DESIGN OF THE FORMATION MAINTENANCE CONTROLLER

As there is no obvious coupling between the vertical and horizontal position channels of the UAV, the vertical position channel of the UAV needs to be considered separately. The height control subsystem function for the pursuer is set as $\dot{z}_p = v_{p_z}$. The relative position error of the pursuer in z-axis in the herding phase is set as $e_z = \Delta z = \lambda_z^d - \lambda_z$. For the vertical channel, which is fully decoupled from the horizontal channel, we use PID control method for the design. It is straightforward to obtain the desired velocity signal required for the vertical channel when the pursuer is tracking the evader in flight as

$$v_{p_z} = k_p e_z + k_i \int_0^t e_z \, dt + k_d \dot{e}_z \tag{21}$$

From Fig. 3, it can be seen that the specific position of the evader and the relative distance between the evader and the pursuer in the herding phase are known, and the expected v_p and ω_p of the pursuer can be used as the reference velocity of the formation as a whole to achieve the design of formation maintenance in the herding phase. Due to the non-linear feature of the error system, the backstepping method is chosen here for the controller design of the pursuer's forward flight speed and heading angular velocity. As the error system model of the pursuer does not have a strict form of feedback, PID control is used for the design of the channels that do not have the conditions for backstepping.

When the linear and angular velocities of the evader in the formation are known, the v_p and ω_p of the pursuer determine the magnitude of e_x and e_y, and the ω_p of the pursuer can reflect the actual angular deviation of the heading between the evader and the pursuer in the formation in the herding phase. From Eq. (13), it can be seen that when $\omega_e \neq 0$, the desired flight trajectory of the evaders in 3D space is curved, and the analysis conducted through the error system shows that the election of $e_x = \left(\omega_e^{-1}\right) \cdot \left(f_2 + k_1 e_y\right)$. When $e_\varphi = 0$ and the control parameter $k_1 > 0$, the dynamic error of Eq. (13) is $e_y \to 0$. Therefore, the

relative kinematic model of the pursuer and evader within the formation in the *x-o-y* plane can be translated into a strict feedback property. The backstepping method is used to design a suitable control law for v_p and ω_p in formation maintenance. Firstly, we define a new error variable

$$\sigma = e_x - \omega_e^{-1}\left(f_2 + ke_y\right) \tag{22}$$

Substituting Eq. (22) into Eq. (13) gives

$$\dot{e}_y = -\omega_e\sigma - ke_y - v_p \sin e_\varphi \tag{23}$$

The derivative of Eq. (22) can be obtained as

$$\begin{aligned}\dot{\sigma} &= \dot{e}_x - \dot{\omega}_e^{-1}\left(f_2 + ke_y\right) - \omega_e^{-1}\left(\dot{f}_2 + k\dot{e}_y\right)\\ &= e_y\omega_e - v_p\cos e_\phi + f_1 - \dot{\omega}_e^{-1}\left(f_2 + ke_y\right) - \omega_e^{-1}\left[\dot{f}_2 + k\left(-ke_y - \omega_e z - v_p\sin e_\phi\right)\right]\end{aligned} \tag{24}$$

where $\dot{\omega}_e^{-1}$ denotes the first order derivative of ω_e^{-1} with respect to time. To ensure that the formation structure does not change at the herding stage, we need the following theorem.

Theorem 1. *Consider the following Lyapunov function*

$$\begin{aligned}V &= \frac{1}{2}\left(e_y^2 + \sigma^2 + e_\varphi^2\right)\\ &= V_1 + \frac{1}{2}e_\varphi^2\end{aligned} \tag{25}$$

where V_1 belongs to the invariant set $\mathcal{M}$, there exists desired ω_p and v_p

$$\omega_p = \omega_e - k_\varphi e_\varphi - k_{\varphi 1}\dot{e}_\varphi - k_{\varphi 2}\int_0^t e_\varphi\, dt \tag{26}$$

$$\begin{aligned}v_p &= k_2\sigma + e_y\left(k_1^2\omega_e^{-1} - k_1\dot{\omega}_e^{-1}\right) + f_1 - \dot{\omega}_e^{-1}f_2 - \omega_e^{-1}\dot{f}_2\\ &= k_2 e_x + e_y\left(k_1^2\omega_e^{-1} - k_1\dot{\omega}_e^{-1} - k_1k_2\omega_e^{-1}\right) + f_1 - \dot{\omega}_e^{-1}f_2 - \omega_e^{-1}\dot{f}_2 - k_2\omega_e^{-1}f_2\end{aligned} \tag{27}$$

to satisfy the (asymptotic) stability requirement of the relative dynamic system of the formation (Eq.13), where $k_2 > k_1 > 0$.

Proof. Substituting Eqs. (13), (22), (23), and (24) into (25), we obtain

$$\begin{aligned}\dot{V} &= e_y\dot{e}_y + \sigma\dot{\sigma} + e_\varphi\dot{e}_\varphi\\ &= -ke_y^2 + \sigma\left[v_p\left(-\cos e_\varphi + k\omega_e^{-1}\sin e_\varphi - e_y\sigma^{-1}\sin e_\varphi\right) + k\sigma\right.\\ &\left. + f_1 + e_y\left(k^2\omega_e^{-1} - k\dot{\omega}_e^{-1}\right) - \dot{\omega}_e^{-1}f_2 - \omega_e^{-1}\dot{f}_2\right] + e_\varphi\left(\omega_e - \omega_p\right)\end{aligned} \tag{28}$$

From Eq. (28), the v_p coefficient expected by the pursuer in the *x-o-y* plane is

$$\eta_p = -\cos e_\varphi + k\omega_e^{-1}\sin e_\varphi - e_y\sigma^{-1}\sin e_\varphi \tag{29}$$

According to Eq. (29), it is clear that by selecting a suitable heading angle error e_φ, the pursuer may expect a v_p factor of zero. Therefore, Eq. (28) does not represent the v_p expected in the formation maintenance controller. Furthermore, it is clear from Eq. (13) that for the pursuer, picking the appropriate ω_p, the heading angle error e_φ can be any value. But in practice, it is that the heading angle error e_φ should be close to zero. Therefore, we assume that when $e_\varphi \to 0$ holds, Eq. (13) can be rewritten as

$$\begin{cases}\dot{e}_x = \omega_e e_y - v_p + f_1\\ \dot{e}_y = -\omega_e e_x + f_2\end{cases} \tag{30}$$

where f_1, f_2 are known finite polynomials. Choosing Eq. (22) as the virtual control input and substituting it into (30) we get

$$\dot{e}_y = -\omega_e\sigma - k_2 e_y \tag{31}$$

Taking the derivative of Eq. (22) and substituting Eq. (31) into it gives

$$\dot{\sigma} = \omega_e e_y - v_p + f_1 - \dot{\omega}_e^{-1}\left(f_2 + ke_y\right) - \omega_e^{-1}\left[\dot{f}_2 + k\left(-\omega_e\sigma - ke_y - v_p\sin e_\varphi\right)\right] \tag{32}$$

and from Eq. (25), the Lyapunov function part V_1 takes the derivative as follows

$$\begin{aligned}\dot{V}_1 &= e_y\dot{e}_y + \sigma\dot{\sigma} \\ &= -k_1 e_y^2 + \sigma\left[-v_p + k_2\sigma + e_y\left(k_1^2\omega_e^{-1} - k_1\dot{\omega}_e^{-1}\right) + f_1 - \dot{\omega}_e^{-1}f_2 - \omega_e^{-1}\dot{f}_2\right]\end{aligned} \tag{33}$$

Substituting Eq. (27) into Eq. (33), we get

$$\begin{aligned}\dot{V}_1 &= e_y\dot{e}_y + \sigma\dot{\sigma} \\ &= -k_1 e_y^2 - (k_2 - k_1)\,\sigma^2 \le 0\end{aligned} \tag{34}$$

In other words, when $e_\varphi \to 0$, we can obtain $\dot{V} \le 0$ and $V > 0$ based on Lemma 2 and 3. On the other hand, the domain of e_y is bounded within the neighbourhood Γ since e_y only contains cos or sin functions and constant terms, which makes sure that Θ is bounded. Hence, Theorem 1 holds. □

When $\omega = 0$, the evader is then moving in a straight line in three dimensions. Therefore, the relative position error of Eq. (13) is simplified to

$$\begin{cases}\dot{e}_x = -v_p\cos e_\varphi + \tilde{f}_1 \\ \dot{e}_y = -v_p\sin e_\varphi + \tilde{f}_2 \\ \dot{e}_\varphi = \omega_p\end{cases} \tag{35}$$

where $\tilde{f}_1 = -\lambda_0\dot{\vartheta}\sin\vartheta + v_e$ and $\tilde{f}_2 = \lambda_0\dot{\vartheta}\cos\vartheta$.

Theorem 2. *Considering the following Lyapunov candidate function*

$$V_2 = \ln(\cosh e_x) + \ln\left(\cosh e_y\right) + \frac{1}{2}e_\varphi^2 \tag{36}$$

When the evader moves in a straight trajectory, there exists desired v_p and ω_p that enable Eq. (35) to satisfy the requirement of asymptotic stability of the system.

Proof. Taking the derivative of Eq. (36) and substituting Eq. (35) into it gives

$$\dot{V}_2 = \left(-v_p\cos e_\varphi + \tilde{f}_1\right)\tanh e_x + \left(-v_p\sin e_\varphi + \tilde{f}_2\right)\tanh e_x + \omega_p e_\varphi \tag{37}$$

set the pursuer's expectation v_p and ω_p in the *x-o-y* plane as

$$v_p = c_1\left(\tanh e_x\cos e_\varphi - \tanh e_y\sin e_\varphi\right) + \xi \tag{38}$$

$$\omega_p = -c_2 e_\varphi - c_3\,\mathrm{sgn}(e_\varphi)\tanh^2(e_y) \tag{39}$$

where $c_1, c_2, c_3 > 0$. Substituting Eqs. (38) and (39) into (37), we get

$$\begin{aligned}\dot{V}_2 = &-c_1\tanh^2(e_x)\cos^2(e_\varphi) - \left[c_3\left|e_\varphi\right| - c_1\sin^2(e_\varphi)\right]\tanh^2(e_y) \\ &+ \xi\left(\tanh e_x\cos e_\varphi + \tanh e_y\sin e_\varphi\right) + \tilde{f}_1\tanh e_x + \tilde{f}_2\tanh e_y - c_2 e_\varphi^2\end{aligned} \tag{40}$$

where $\|\xi\left(\tanh e_x\cos e_\varphi + \tanh e_y\sin e_\varphi\right) + \tilde{f}_1\tanh e_x + \tilde{f}_2\tanh e_y\| \le 2\|\xi\| + \|\tilde{f}_1\| + \|\tilde{f}_2\|$. Further analysis shows that the parameter ξ and η are selected as

$$\xi = -\frac{\tilde{f}_1\tanh e_x + \tilde{f}_2\tanh e_y}{\eta + \tanh e_x\cos e_\varphi + \tanh e_y\sin e\varphi} \tag{41}$$

$$\eta = \begin{cases}0, & \tanh e_x\cos e_\varphi + \tanh e_y\sin e_\varphi \ne 0 \\ \eta_0, & \tanh e_x\cos e_\varphi + \tanh e_y\sin e_\varphi = 0\end{cases} \tag{42}$$

where $\eta_0 > 0$. When the evader is moving on a straight trajectory, f_1,f_2 in Eq. (35) are both bounded numerical terms, so that there must exist $2\|\xi\| + \|\tilde{f}_1\| + \|\tilde{f}_2\| \le \gamma$. Substituting Eq. (41) into (40), when $\eta = 0$

$$\dot{V}_2 = -c_2 e_\varphi^2 - c_1\tanh^2(e_x)\cos^2(e_\varphi) - \left[c_3\left|e_\varphi\right| - c_1\sin^2(e_\varphi)\right]\tanh^2(e_y) \tag{43}$$

when $e_\varphi \to 0$, $\sin^2(e_\varphi) < \left|e_\varphi\right|$ always holds. Therefore, if we choose the appropriate $c_1, c_2, c_3 > 0$, then $\dot{V}_2 \le 0$. When $\eta = \eta_0$, we choose the appropriate η_0, thus $\dot{V}_2 + \gamma \le 0$. □

In summary, when the evader moves in a curve, the control laws designed by Eqs. (26) and (27) can achieve stable driving of the evader by the formation pursuer in the herding phase and maintain the desired formation. When the evader moves in a straight trajectory, the control law designed by Eqs. (38) and (39) can achieve stable driving of the evader by the formation pursuer in the herding phase and maintain the desired formation.

4 | DESIGN OF THE TRAJECTORY TRACKING CONTROLLER

4.1 | Position tracking controller

We set the height error of the evader in tracking the desired trajectory to

$$\begin{cases} e_1 = z_d - z \\ \dot{e}_1 = \dot{z}_d - \dot{z} \end{cases} \tag{44}$$

Theorem 3. *Considering the following Lyapunov function*

$$V(e_1) = \frac{1}{2}\left[e_1^2 + \lambda_1 \left(\int_0^t e_1(\tau)\, d\tau\right)^2\right] \tag{45}$$

where $\lambda_1 > 0$. The evader height tracking subsystem is designed with control input U_1 to satisfy the requirement of Lyapunov's asymptotic stability.

Proof. The derivative of Eq.(45) gives

$$\dot{V}(e_1) = e_1\left[\dot{z}_d - \dot{z} + \lambda_1 \left(\int_0^t e_1(\tau)\, d\tau\right)\right] \tag{46}$$

For Eq.(46), to ensure that $\dot{V}(e_1) \leq 0$, use $\dot{z}$ as the virtual control input and pick the function β_1 as

$$\beta_1 = \dot{z}_d + \lambda_1 \int_0^t e_1(\tau)\, d\tau + c_1 e_1 \tag{47}$$

where $c_1 > 0$. Substituting Eq.(47) into (46), we get $\dot{V}(e_1) = -c_1 e_1^2 < 0$. Although the Lyapunov stability condition is satisfied, it does not ensure that $\dot{z}$ will eventually converge to the set β_1, so the error variable e_2 is set as

$$e_2 = \beta_1 - \dot{z} = \dot{z}_d + \lambda_1 \int_0^t e_1(\tau)\, d\tau + c_1 e_1 - \dot{z} \tag{48}$$

Taking the derivative of Eq.(48) yields

$$\dot{e}_2 = \ddot{z}_d + \lambda_1 e_1 + c_1 \dot{e}_1 - \ddot{z} \tag{49}$$

In order to make $\dot{e}_2 > 0$, the Lyapunov function is chosen from Eq.(47) and (48) as

$$V(e_1, e_2) = \frac{1}{2}\left[e_1^2 + e_2^2 + \lambda_1 \left(\int_0^t e_1(\tau)\, d\tau\right)^2\right] \tag{50}$$

Taking the derivative of Eq.(50) yields

$$\dot{V}(e_1, e_2) = e_1\left(\dot{e}_1 + \lambda_1 \int_0^t e_1(\tau)\, d\tau\right) + e_2 \dot{e}_2 \tag{51}$$

From Eq.(44) and (48), it follows that

$$\dot{e}_1 = \dot{z}_d - \dot{z} = e_2 - \lambda_1 \int_0^t e_1(\tau)\, d\tau - c_1 e_1 \tag{52}$$

Substituting Eq.(49) and (52) into (51) gives

$$\dot{V}(e_1, e_2) = -c_1 e_1^2 + e_2 \left[\left(1 - c_1^2 + \lambda_1\right) e_1 + c_1 e_2 + \ddot{z}_d - c_1 \lambda_1 \int_0^t e_1(\tau)\, d\tau - \ddot{z} \right] \tag{53}$$

From Eq.(6), $\ddot{z}$ is a function on U_1. To ensure $\dot{V}(e_1, e_2) \leq 0$, the control input for the evader height tracking subsystem is chosen as

$$U_1 = \eta \left[g - \ddot{z}_d - \left(1 - c_1^2 + \lambda_1\right) e_1 - (c_1 + c_2)\, e_2 + c_1 \lambda_1 \int_0^t e_1(\tau)\, d\tau \right] \tag{54}$$

where $\eta = \frac{m}{\cos\varphi \cos\theta}$ and $c_2 > 0$. And we get $\dot{V}(e_1, e_2) = -c_1 e_1^2 - c_2 e_2^2 \leq 0$. □

From Eq.(6), the height control input U_1 of the evader and the intermediate control quantities u_x and u_y of the roll and pitch channels form its dynamic equations in x-axis and y-axis. Therefore, similar to the height error of the system, the position error in the horizontal direction is set to

$$\begin{cases} e_3 = x_d - x \\ e_5 = y_d - y \end{cases} \tag{55}$$

From Eq.(44) and Theorem 3, it follows that, similar to the height error variable of the system, the error variable in the horizontal direction is

$$\begin{cases} e_4 = \dot{x}_d + \lambda_2 \int_0^t e_3(\tau)\, d\tau + c_3 e_3 - \dot{x} \\ e_6 = \dot{y}_d + \lambda_3 \int_0^t e_5(\tau)\, d\tau + c_5 e_5 - \dot{y} \end{cases} \tag{56}$$

The evader's horizontal position control input u_x and u_y is designed to satisfy Lyapunov's asymptotic stability, thus

$$\begin{aligned} u_x &= \frac{m}{U_1} \left[-\ddot{x}_d - \left(1 - c_3^2 + \lambda_2\right) e_3 - (c_3 + c_4)\, e_4 + c_3 \lambda_2 \int_0^t e_3(\tau)\, d\tau \right] \\ u_y &= \frac{m}{U_1} \left[-\ddot{y}_d - \left(1 - c_5^2 + \lambda_3\right) e_5 - (c_5 + c_6)\, e_6 + c_5 \lambda_3 \int_0^t e_5(\tau)\, d\tau \right] \end{aligned} \tag{57}$$

where $c_3, c_4, \lambda_2 > 0$ and $c_5, c_6, \lambda_3 > 0$.

4.2 | Attitude tracking controller

We set the yaw error of the evader in tracking the desired trajectory to

$$\begin{cases} e_7 = \psi_d - \psi \\ \dot{e}_7 = \dot{\psi}_d - \dot{\psi} \end{cases} \tag{58}$$

Theorem 4. *Considering the following Lyapunov function*

$$V(e_7) = \frac{1}{2} \left[e_7^2 + \lambda_4 \left(\int_0^t e(\tau)\, d\tau \right)^2 \right] \tag{59}$$

where $\lambda_4 > 0$. The evader yaw control subsystem is designed with control input U_4 to satisfy the requirement of Lyapunov's asymptotic stability.

Proof. Similar to Theorem 3, we ensure that $\dot{V}(e_7) \leq 0$, use $\dot{\psi}$ as the virtual control input and pick the function α_1 as $\alpha_1 = \dot{\psi}_d + \lambda_4 \int_0^t e_7(\tau)\, d\tau + c_7 e_7$ and set the error variable $e_8 = \alpha_1 - \dot{\psi} = \dot{\psi}_d + \lambda_4 \int_0^t e_7(\tau)\, d\tau + c_7 e_7 - \dot{\psi}$. According to the height tracking control subsystem in the evader model, to ensure that e_8 is positive, the Lyapunov function is chosen as $V(e_7, e_8) = \frac{1}{2} \left[e_7^2 + e_8^2 + \lambda_4 \left(\int_0^t e_7(\tau)\, d\tau \right)^2 \right]$. The derivative of this equation gives

$$\dot{V}(e_7, e_8) = -c_7 e_7^2 + e_8 \left[\left(1 - c_7^2 + \lambda_4\right) e_7 + c_7 e_8 + \ddot{\psi}_d - c_7 \lambda_4 \int_0^t e_7(\tau)\, d\tau - \ddot{\psi} \right] \tag{60}$$

where $\ddot{\psi} = \dot{\theta}\dot{\phi}\left(\frac{J_x - J_y}{J_z}\right) + \frac{1}{J_z}U_4$ from Eq.(6). Therefore, we set the yaw control input U_4 to

$$U_4 = J_z\left[-\dot{\theta}\dot{\phi}\left(\frac{J_x - J_y}{J_z}\right) + \ddot{\psi}_d + \left(1 - c_7^2 + \lambda_4\right)e_7 + (c_7 + c_8)\,e_8 - c_7\lambda_4\int_0^t e_7(\tau)\,d\tau\right] \tag{61}$$

where $c_7, c_8, \lambda_4 > 0$. Obviously, this makes $\dot{V}(e_7, e_8) = -c_7e_7^2 - c_8e_8^2 \leq 0$ holds. □

The yaw angle of the evader is determined by τ_3. When the design of the yaw and horizontal position controller for the system is completed, the control inputs for its roll and pitch are determined by u_x and u_y. From Eq.(6), when the evader is tracking the desired trajectory its desired roll and pitch angles are $\phi_d = \arcsin\left(u_x\sin\psi_d - u_y\cos\psi_d\right)$ and $\theta_d = \arcsin\left(\frac{u_x\sin\psi_d + u_y\cos\psi_d}{\cos\phi_d}\right)$.

Based on Eq.(56) and (57), the design was carried out using the integral backstepping method, setting its roll and pitch attitude error to

$$\begin{cases} e_9 = \phi_d - \phi \\ e_{10} = \dot{\phi}_d + \lambda_5\displaystyle\int_0^t e_9(\tau)\,d\tau + c_9e_9 - \dot{\phi} \\ e_{11} = \theta_d - \theta \\ e_{12} = \dot{\theta}_d + \lambda_6\displaystyle\int_0^t e_{11}(\tau)\,d\tau + c_{11}e_{11} - \dot{\theta} \end{cases} \tag{62}$$

The control inputs U_2 for the roll and U_3 for the pitch of the evader are designed to satisfy Lyapunov's asymptotic stability, thus

$$\begin{aligned} U_2 &= J_x\left[-\dot{\theta}\dot{\psi}\left(\frac{J_y - J_z}{J_x}\right) - \Omega_g\dot{\theta}\frac{J_r}{J_x} + \ddot{\phi}_d + \left(1 - c_9^2 + \lambda_5\right)e_9 + (c_9 + c_{10})\,e_{10} - c_9\lambda_5\int_0^t e_9(\tau)\,d\tau\right] \\ U_3 &= J_y\left[-\dot{\phi}\dot{\psi}\left(\frac{J_z - J_x}{J_y}\right) - \Omega_g\dot{\phi}\frac{J_r}{J_y} + \ddot{\theta}_d + \left(1 - c_{11}^2 + \lambda_6\right)e_{11} + (c_{11} + c_{12})\,e_{12} - c_{11}\lambda_6\int_0^t e_{11}(\tau)\,d\tau\right] \end{aligned} \tag{63}$$

where $c_9, c_{10}, c_{11}, c_{12}, \lambda_5, \lambda_6 > 0$.

4.3 | Collision avoidance potential function

To ensure the safety of each UAV's flight, it is assumed that the UAV can detect obstacles within its sensing area. Since it is necessary to use both attractive forces to enable the relative aggregation of UAVs within the formation and repulsive forces to avoid collisions, we propose to add a transition area between attractive and repulsive potential edges by means of dynamic adjustment factors α and β. When the repulsive adjustment factor is too small, the UAV may not be able to avoid obstacles due to too little repulsion; when the attractive adjustment factor is too small or the repulsive adjustment factor is too large, it will result in unknown chattering of the final obstacle avoidance trajectory. To address the above problems, the adaptive potential function is designed. The attractive transition region makes the attractive force on the UAV decrease gradually with the distance between the UAV and the obstacle, so as to achieve the purpose of safe obstacle avoidance. The repulsive transition region makes the UAV have more space to adjust its direction and improve the chattering problem of the obstacle avoidance trajectory.

The established potential function combined with distributed control law is then used to generate trajectories for each UAV tracking without any collisions. The method allows a virtual potential field to exist around each UAV in the formation, and each UAV will converge to a steady state at inter-aircraft distances under the combined forces of attraction and repulsion. For the *i*-th UAV, the repulsive potential function $U_{rep,i}$ can be described as:

$$U_{rep,i} = \begin{cases} \dfrac{1}{2}\alpha k_{rep}\left(\dfrac{1}{\rho_{io}} - \dfrac{1}{d_o}\right)^2 & \rho_{io} \leq d_1 \\ 0 & \rho_{io} > d_1 \end{cases} \tag{64}$$

where k_{rep} denotes the gain coefficients of the repulsive function. As shown in Fig. 4, for a spherical obstacle O_k of radius R_o centred on c_k, ρ_{io} is the distance from UAV i to c_k, d_o denotes the influence range of the obstacle, d_1 is the influence range of the

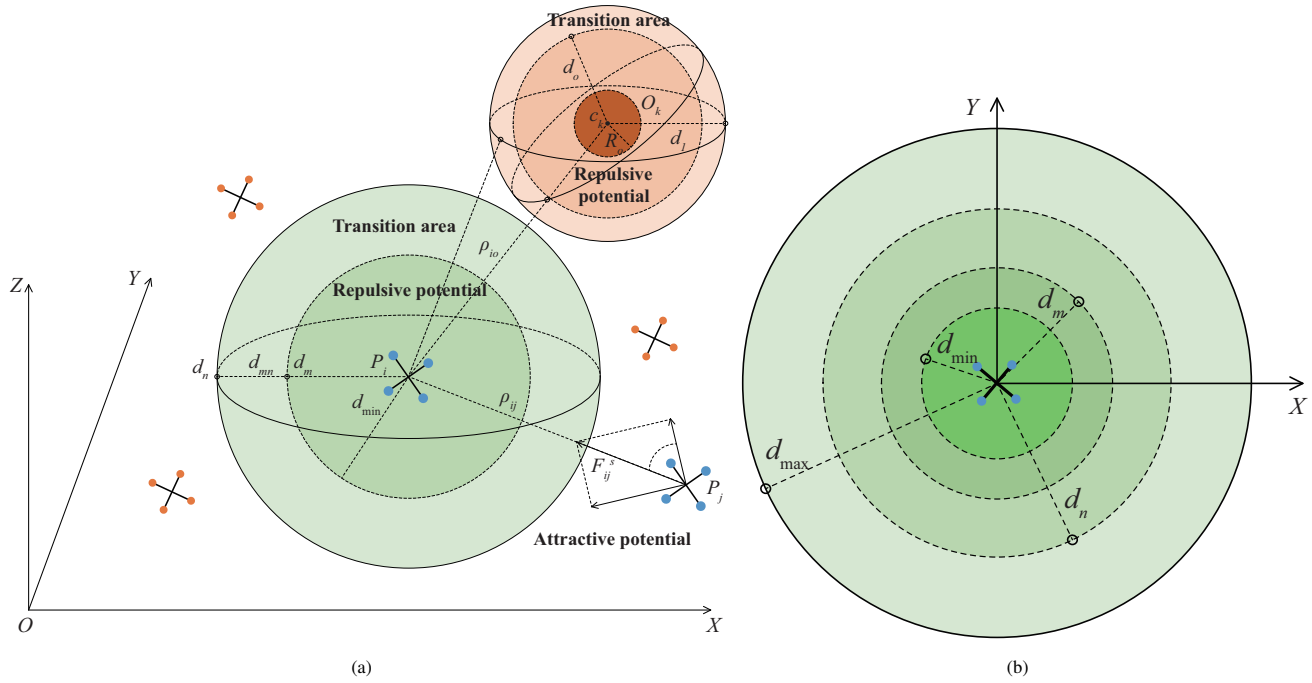

FIGURE 4 (a) Representation of virtual forces between virtual obstacles and UAVs. (b) Cross-sectional diagram of the UAV potential area.

obstacle in the increased transition area. The dynamic adjustment factor α added to the repulsive function is defined as:

$$\alpha = \begin{cases} 1 & \rho_{io} < d_o \\ \frac{1}{2}\left[1 + \cos\left(\frac{2(\rho_{io} - d_o)}{R_o}\pi\right)\right] & d_o \le \rho_{io} < d_1 \\ 0 & \rho_{io} \ge d_1 \end{cases} \tag{65}$$

We then describe the attractive potential function as

$$U_{att,i} = \frac{1}{2}\beta k_{att}\rho_{ij}^2 \tag{66}$$

where dynamic adjustment factor β added to the attractive function is

$$\beta = \begin{cases} 0 & \rho_{io} < R_o \\ \frac{1}{2}\left[1 + \sin\left(\frac{2(\rho_{io} - R_o)}{R_o}\pi - \frac{\pi}{2}\right)\right] & R_o \le \rho_{io} < d_o \\ 1 & \rho_{io} \ge d_o \end{cases} \tag{67}$$

where $U_{att,i}$ denotes attractive potential. k_{att} denotes the gain coefficients of the attractive function. If the position coordinates of the i-th UAV is $P_i = [x_i, y_i, z_i]^T$, then $\rho_{ij} = \|P_i - P_j\|$ denotes the Euclidean distance between UAV i and UAV j.

Let the desired distance between neighbouring UAVs in the formation be $d_{mn} \in [d_m, d_n]$. The virtual forces between the UAVs in the formation are divided into inter-agent repulsive forces and inter-agent attractive forces. The inter-agent repulsion causes neighbouring UAVs in the formation to move away from each other to avoid collisions between the aircraft. Inter-agent attraction brings neighbouring UAVs in a formation closer together to avoid formation break-up. The inter-agent virtual force F_{ij}^s between

UAV i and j is defined as:

$$\vec{F}_{ij}^{s} = \begin{cases} \sum_{j=1, j\neq i}^{n} k_{ij} \left(\frac{1}{\rho_{ij}} - \frac{1}{d_m} \right) \left(P_i - P_j \right) & d_{\min} < \rho_{ij} < d_m \\ \sum_{j=1, j\neq i}^{n} k_{ij} \left(P_i - P_j - P_{ij} \right) & d_m \leq \rho_{ij} \leq d_n \\ \sum_{j=1, j\neq i}^{n} k_{ij} \left(\frac{1}{d_{\max} - d_n} - \frac{1}{d_{\max} - \rho_{ij}} \right) \left(P_i - P_j \right) & d_n < \rho_{ij} < d_{\max} \end{cases} \tag{68}$$

where d_{min} denotes the minimum safe distance between each UAV in the formation, k_{ij} is the unit direction vector from i to j. As illustrated in Fig. 4. When other UAVs are present in the UAV area within the formation, the UAVs will adjust their distance with respect to other UAVs in the field of action according to the pre-defined rules of inter-agent virtual force, effectively avoiding collisions while maintaining the formation and achieving pursuer to evader trajectory tracking in the herding phase. When the formation is not in the influence range of the obstacle, the virtual force within the formation is dominant, and the formation reaches stability with $\|P_i - P_j - P_{ij}\| \to 0$. When $d_{\min} < \rho_{ij} < d_m$, UAV j is in the repulsive domain of UAV i. Meanwhile, the virtual force between UAV i and j is expressed as repulsive force, and the two UAVs will move away from each other. When $\rho_{ij} = d_{\min}$, the repulsive action is at its maximum. When $\rho_{ij} = d_m$, $F_{ij}^{s} = 0$. When $d_m < \rho_{ij} < d_n$, UAV j is in the stability domain of UAV i. When $d_n < \rho_{ij} < d_{\max}$, UAV j is in the attractive domain of UAV i. At this point the virtual force between the two UAVs is expressed as attractive force and two UAVs will approach each other. When $\rho_{ij} = d_n$, $F_{ij}^{s} = 0$. When $\rho_{ij} = d_{\max}$, the attractive force between the formation UAVs is at its maximum.

Inside the formation, UAV i is affected by the virtual forces of other UAVs within the potential range. Outside the formation, it is subject to the virtual potential field forces of other formation UAVs and obstacles. The virtual combined force on UAV i in space is therefore expressed as

$$\vec{F}_i^{total} = \varrho_i \vec{F}_{ij}^{s}(\rho_{ij}) + \varsigma_i \left[k_1 \vec{F}_{att,i}(\rho_{ij}) + k_2 \vec{F}_{rep,i}(\rho_{ij}) \right] \tag{69}$$

where $\varrho_i, \varsigma_i, k_1, k_2$ denote the control parameters and have $\varrho_i \neq 0$ for any one UAV i in the formation, and $\vec{F}_{att,i}(\rho_{ij})$, $\vec{F}_{rep,i}(\rho_{ij})$ are determined by the potential functions. The design of the obstacle avoidance potential function is followed by effective modulation of the velocity vector of each UAV, thereby enabling cooperative obstacle avoidance control of the UAV formation. For this, the desired velocity vector of UAV i is set as $\vec{V}_i = \vec{F}_i^{total}$. The desired velocity of UAV i is decomposed by in the x, y and z axes to give V_i^x, V_i^y, V_i^z, which are the desired velocity components in each axis, respectively. We translates this velocity component into the speed, heading and pitch control required for the actual flight of each UAV in the formation, which are expressed as

$$\begin{cases} V_i = \sqrt{(V_i^x)^2 + (V_i^y)^2 + (V_i^z)^2} \\ \psi_i = \arctan \dfrac{V_i^y}{V_i^x} \\ \theta_i = \arctan \dfrac{V_i^z}{V_i^x} \end{cases} \tag{70}$$

The formation achieves cooperative collision avoidance when UAV i in the formation enters the range of an obstacle or neighbouring UAV j's potential area, and all other UAVs in the formation are in the stable domain. The velocity components of UAV i in x, y and z axes are

$$\begin{cases} V_i^x = \varrho_i \sum_{j=1}^{n} k_{ij} \left(x_i - x_j - \rho_{ij,x} \right) + \varsigma_i \left[k_1 \sqrt{\mu_s^2 + (\mu_t - 1)^2} F_{att,i}^x + k_2 F_{rep,i}^x \right] \\ V_i^y = \varrho_i \sum_{j=1}^{n} k_{ij} \left(y_i - y_j - \rho_{ij,y} \right) + \varsigma_i \left[k_1 \sqrt{\mu_s^2 + (\mu_t - 1)^2} F_{att,i}^y + k_2 F_{rep,i}^y \right] \\ V_i^z = \varrho_i \sum_{j=1}^{n} k_{ij} \left(z_i - z_j - \rho_{ij,z} \right) + \varsigma_i \left[k_1 \sqrt{\mu_s^2 + (\mu_t - 1)^2} F_{att,i}^z + k_2 F_{rep,i}^z \right] \end{cases} \tag{71}$$

where μ_t denotes the time perturbation factor of attraction. When the speed of the UAV is above a certain threshold, μ_t is zero, and when the speed of the UAV is maintained under a specific value for a certain period of time, μ_t denotes the integral function of

time, which is expressed as $\mu_t = \int_{t_0}^{t} \varepsilon \, dt, t > t_0$, and $\frac{d\rho}{dt} < v_0$. When the obstacle is in the middle of the formation's neighbouring UAVs, a random force μ_s is added to prevent collision that may be detected when the UAVs are constantly approaching the obstacle, where $\mu_s = \int_{t_0}^{t} \xi \, dt, t > t_0$ and $\frac{d\rho}{dt} < v_0$.

5 | SIMULATION

In this section, the simulation is conducted to verify the effectiveness of the proposed framework and method. We provide the simulation results of both staged of seeking and pursuing. During the initial seeking process, the pursuers seek the distant evaders. After satisfying the relative distance between the pursuers and the evader, the pursuing phase is initiated so that the pursuers drive the evader to the target area. Then we extend the pursuing phase to the three-dimensional environment to show the stability and superiority of the proposed method.

A. 2D environment

The simulation results of two stages are shown in Fig. 5. At the seeking stage, two sets of pursuers find and approach the evaders as shown in Fig. 5(a). After entering the pursuing phase, two groups of pursuers successfully drive the evaders to the designated areas S_1 and S_2 in a complex environment with various obstacles in a two dimensional space, as shown in Fig. 5(b).

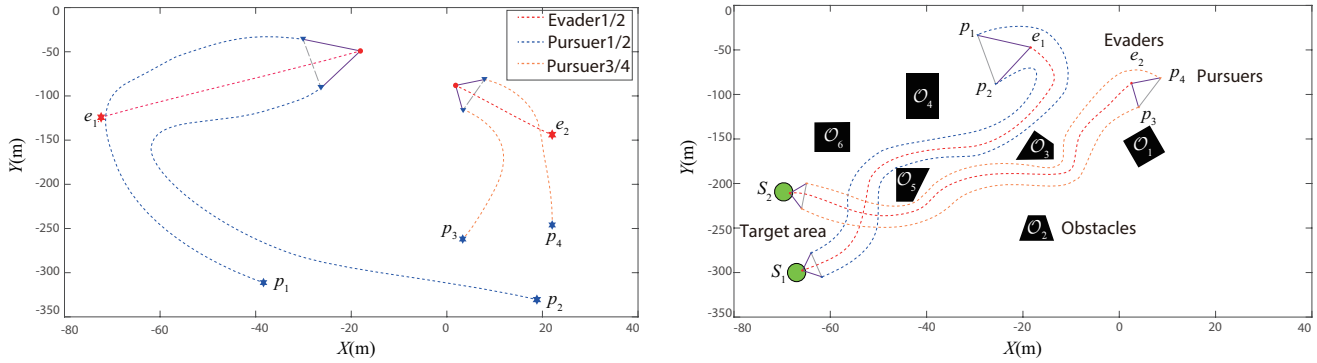

(a) Seeking stage

(b) Pursuing stage

FIGURE 5 Snapshots of the paths of the UAVs in two dimensional space.

B. 3D environment

Consider a set of quadrotor UAVs ($e = 1$ evader and $p = 2$ pursuers) in three dimensional environment, where the mass of each UAV is set to be $m = 0.76$ kg, the initial state of the evader is chosen to be $v_e = 0.54\pi$ m/s and $\omega_e = 0.27\pi$ rad/s. Meanwhile, the normal repulsive force influence range of each UAV and obstacle was set to $d_0 = 30$, and the designed repulsive force influence range $d_1 = 40$. The parameters $k_{rep} = 8$, $k_{att} = 4$, perturbation factor $\varepsilon = 3$, and random force factor $\xi = 8$. The sinusoidal disturbances were applied to each UAV.

At the pursuing stage, the pursuer drives the evader to the target location, and the motion of the desired trajectory for the evader (labeled 0) is set as

$$\begin{cases} x_0 = 4\cos(0.27\pi t) \\ y_0 = 4\sin(0.27\pi t) \\ z_0 = -0.27t \end{cases}$$

The initial position of the UAV is denoted as $[x, y, z, \varphi]$, i.e., $[2, 0, 0, \pi/6]$ for the evader, $[-0.5, -1, 0, \pi/10]$ for pursuer 1, and $[-2, 2, 0, \pi/14]$ for pursuer 2. The flight space is deployed with two obstacles, two of which are spherical obstacles located at $c_1 = [0, 0, -1.5]$ and $c_2 = [0, 0, -6.5]$, respectively, with radius $R_o = 2$ m.

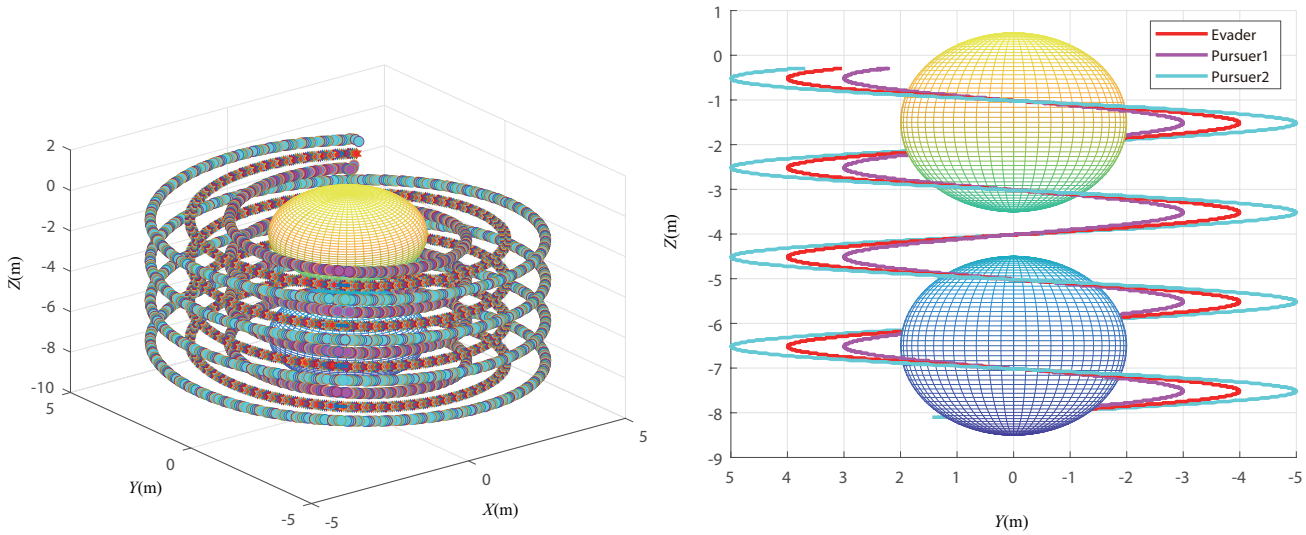

(a) Flight trajectories of three UAVs in the three dimensional environment

(b) Flight trajectories of three UAVs in the YZ plane

FIGURE 6 Flight trajectories of three UAVs.

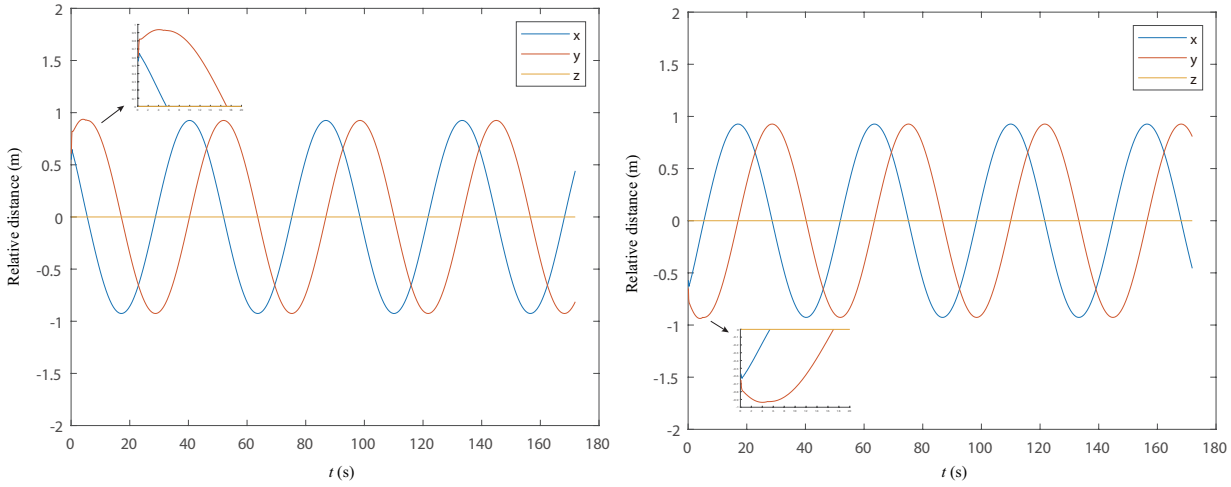

(a) The relative distance between pursuing UAV 1 and evading UAV

(b) The relative distance between pursuing UAV 2 and evading UAV

FIGURE 7 The relative distance curve between pursuing UAVs and evading UAV.

Figure. 6 shows the flight trajectories of the proposed collision-free formation control strategy for three (2 pursuers, 1 evader) quadrotor UAVs in 3D space, where the outermost blue and innermost purple trajectories represent the trajectories of the pursuers, and the middle trajectory represents the evader's trajectory. Two spherical obstacles were placed in the flight space. Figs. 7(a) and 7(b) provide the relative distance curves between the pursuers and the evader. It can be observed that it takes about 9s to complete a stable pursuing of the trajectory. Since the positions of each UAV are vectors with directions, the sum of the position vectors in x, y, and z axes is constant at any time after 9s. Figures. 8(a) and 8(b) show the velocity change curves of the pursuers 1 and 2, respectively. The figures show that the speed of each pursuing UAV can finally reach stability around 9s.

Take pursuing UAV 1 as an example to illustrate the effectiveness of the designed control law. In Fig. 9(a), the tracking error trajectories of pursuing UAV 1 in x, y and z axis are shown. During the initial flight, the pursuing UAV 1 adjusts its state and senses any obstacles around it. During this time, the tracking error trajectory fluctuates due to the need to avoid collisions with obstacles or nearby UAVs. At this point, each pursuing UAV is able to maintain a pre-determined formation, matching the desired relative distance and trajectory. Fig. 9(b) illustrates the tracking error trajectories of pursuing UAV 1 with the addition of a sinusoidal perturbation. As we can observe, over time, the designed control law is effective under uncertainties. As for the evader

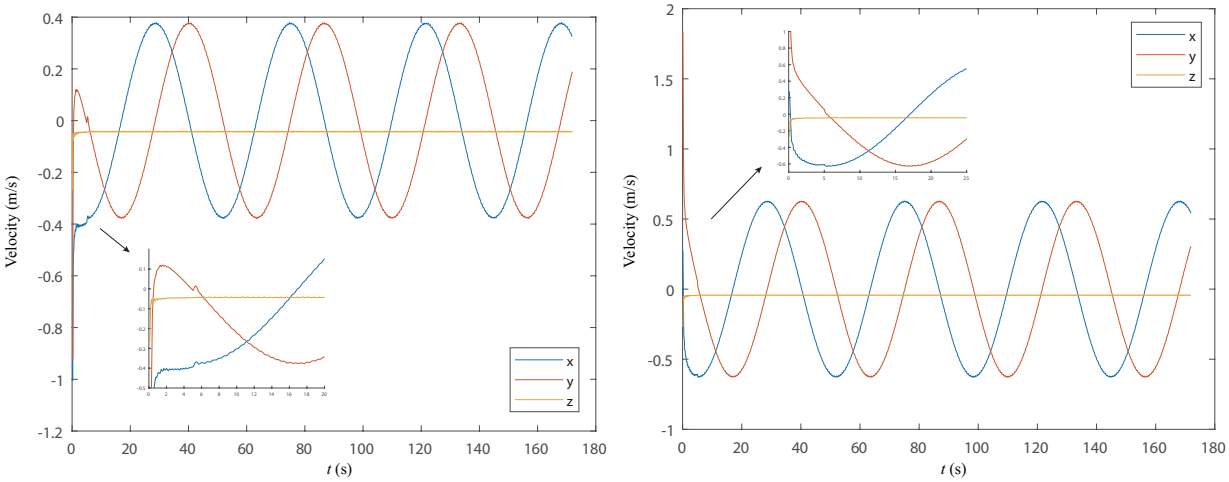

(a) The velocity change curves of pursuing UAV 1

(b) The velocity change curves of pursuing UAV 2

FIGURE 8 The velocity change curves of pursuing UAV 1 and 2.

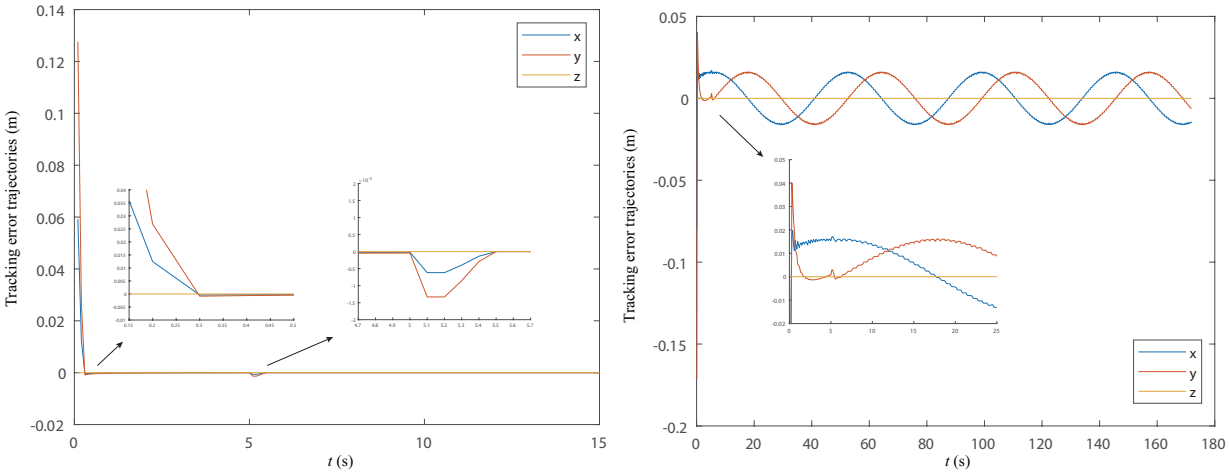

(a) Tracking error trajectories of pursuing UAV 1 in the general case

(b) Tracking error trajectories of pursuing UAV 1 with the addition of sinusoidal perturbation

FIGURE 9 Tracking error trajectories of pursuing UAV 1 in different cases.

shown in Fig. 10, it can be observed that the trajectory converges to the desired one, showing that the goal of herding is achieved. Finally, The result of attitude control is shown in Fig. 11, which also shows the effectiveness of the whole control scheme.

From the simulation results it can be observed that under the proposed framework and control scheme, the pursuing UAVs are able to seek, pursue and eventually drive the evading UAVs to the designated target or along the desired trajectory while avoiding collisions. In addition, all pursuing UAVs achieve asymptotic tracking in the presence of unknown disturbances and uncertainties, and the controllers converge stably using the control scheme in the developed collision avoidance formation during the pursuing process.

6 | CONCLUSION

In this paper, a novel collision-free pursuit-evasion framework is proposed to solve the herding and formation control problem of a group of non-cooperative quadrotor UAVs in the presence of uncertain disturbances. First, the desired trajectory of the formation evader is set and used as the initial actual trajectory. The pursuit-evasion problem is decomposed into whether the

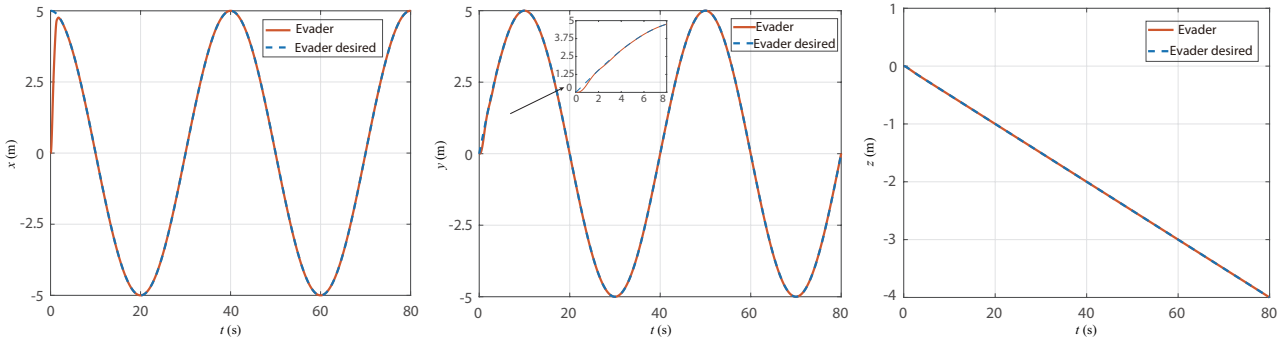

(a) The position error of the evading UAV in x axis (b) The position error of the evading UAV in y axis (c) The position error of the evading UAV in z axis

FIGURE 10 The position error of the evading UAV

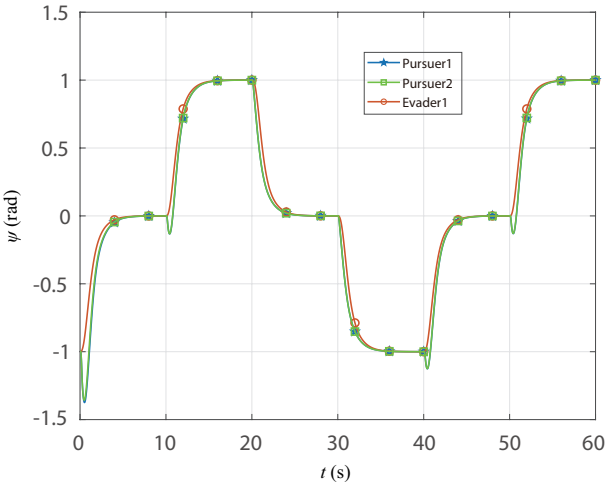

FIGURE 11 The attitude tracking curves of yaw angles

pursuer can find and approach the evaders at the seeking stage and drive the evaders to follow the desired trajectory while maintaining the formation at the pursuing stage. The formation maintenance controller and trajectory tracking controller are designed and the collision avoidance potential function is established to ensure collision avoidance with other UAVs or obstacles. The stability of the entire closed-loop system was provided using Lyapunov's theorem. The stability analysis and simulation results for three UAVs show that the proposed framework achieves the goal of herding formation and collision avoidance in a pursuit-evasion scenario under uncertainties and external disturbances.

CONFLICT OF INTEREST

The authors declare no potential conflict of interests.

REFERENCES

1. Cao Y, Yu W, Ren W, Chen G. An overview of recent progress in the study of distributed multi-agent coordination. *IEEE Transactions on Industrial informatics.* 2012;9(1):427–438.
2. Shlapatskyi V, Kamak YO, Andriyenko O, Zhurahov V, Domanov I, Loginov V. A fault tree of unmanned aircraft systems for military applications. In: IEEE 4th International Conference Actual Problems of Unmanned Aerial Vehicles Developments (APUAVD). 2017:104–107.
3. Ren W, Beard RW, Atkins EM. Information consensus in multivehicle cooperative control. *IEEE Control Systems Magazine.* 2007;27(2):71-82.
4. Wilson S, Pavlic TP, Kumar GP, Buffin A, Pratt SC, Berman S. Design of ant-inspired stochastic control policies for collective transport by robotic swarms. *Swarm Intelligence.* 2014;8:303–327.
5. Sargolzaei A, Abbaspour A, Crane CD. Control of cooperative unmanned aerial vehicles: review of applications, challenges, and algorithms. *Optimization, Learning, and Control for Interdependent Complex Networks.* 2020:229–255.
6. Ye F, Dong H, Lu Y, Zhang W. Consensus controllers for general integrator multi-agent systems: analysis, design and application to autonomous surface vessels. *IET Control Theory & Applications.* 2018;12(5):669–678.

7. Muslimov TZ, Munasypov RA. Consensus-based cooperative control of parallel fixed-wing UAV formations via adaptive backstepping. *Aerospace science and technology.* 2021;109:106416.
8. Peng Z, Wang D, Li T, Han M. Output-feedback cooperative formation maneuvering of autonomous surface vehicles with connectivity preservation and collision avoidance. *IEEE transactions on cybernetics.* 2019;50(6):2527–2535.
9. Wang W, Liang H, Pan Y, Li T. Prescribed performance adaptive fuzzy containment control for nonlinear multiagent systems using disturbance observer. *IEEE Transactions on Cybernetics.* 2020;50(9):3879–3891.
10. Chen L, Duan H. Collision-free formation-containment control for a group of UAVs with unknown disturbances. *Aerospace Science and Technology.* 2022;126:107618.
11. Mahfouz M, Hafez AT, Ashry M, Elnashar G. Formation configuration for cooperative multiple UAV via backstepping PID controller. In: AIAA SPACE and Astronautics Forum and Exposition. 2018:5282.
12. Zhou W, Wang Y, Ahn CK, Cheng J, Chen C. Adaptive fuzzy backstepping-based formation control of unmanned surface vehicles with unknown model nonlinearity and actuator saturation. *IEEE Transactions on Vehicular Technology.* 2020;69(12):14749–14764.
13. Zhang Q, Liu HH. UDE-based robust command filtered backstepping control for close formation flight. *IEEE Transactions on Industrial Electronics.* 2018;65(11):8818–8827.
14. Yang W, Shi Z, Zhong Y. Robust backstepping non-smooth practical tracking for nonlinear systems with mismatched uncertainties. *International Journal of Robust and Nonlinear Control.* 2022;32(6):3674–3695.
15. Kartal Y, Subbarao K, Dogan A, Lewis F. Optimal game theoretic solution of the pursuit-evasion intercept problem using on-policy reinforcement learning. *International Journal of Robust and Nonlinear Control.* 2021;31(16):7886–7903.
16. Ren W, Cao Y. *Distributed Coordination of Multi-Agent Networks: Emergent Problems, Models, and Issues*. Springer Publishing Company, Incorporated, 2013.
17. Chen M, Zhou Z, Tomlin CJ. Multiplayer Reach-Avoid Games via Pairwise Outcomes. *IEEE Transactions on Automatic Control.* 2017;62(3):1451-1457.
18. Garcia E, Casbeer DW, Pachter M. Design and Analysis of State-Feedback Optimal Strategies for the Differential Game of Active Defense. *IEEE Transactions on Automatic Control.* 2019;64(2):553-568.
19. Approximate optimal influence over an agent through an uncertain interaction dynamic. *Automatica.* 2021;134:109913.
20. Pierson A, Schwager M. Controlling noncooperative herds with robotic herders. *IEEE Transactions on Robotics.* 2017;34(2):517–525.
21. Licitra RA, Bell ZI, Dixon WE. Single-agent indirect herding of multiple targets with uncertain dynamics. *IEEE Transactions on Robotics.* 2019;35(4):847–860.
22. Deptula P, Bell ZI, Zegers FM, Licitra RA, Dixon WE. Single agent indirect herding via approximate dynamic programming. In: IEEE Conference on Decision and Control (CDC). 2018:7136–7141.
23. Nardi S, Mazzitelli F, Pallottino L. A game theoretic robotic team coordination protocol for intruder herding. *IEEE Robotics and Automation Letters.* 2018;3(4):4124–4131.
24. Ghommam J, Saad M, Mnif F, Zhu QM. Guaranteed performance design for formation tracking and collision avoidance of multiple USVs with disturbances and unmodeled dynamics. *IEEE Systems Journal.* 2020;15(3):4346–4357.
25. Lyu Y, Hu J, Chen BM, Zhao C, Pan Q. Multivehicle Flocking With Collision Avoidance via Distributed Model Predictive Control. *IEEE Transactions on Cybernetics.* 2021;51(5):2651-2662.
26. Santos MCP, Rosales CD, Sarcinelli-Filho M, Carelli R. A novel null-space-based UAV trajectory tracking controller with collision avoidance. *IEEE/ASME Transactions on Mechatronics.* 2017;22(6):2543–2553.
27. Wang L, Ames AD, Egerstedt M. Safety Barrier Certificates for Collisions-Free Multirobot Systems. *IEEE Transactions on Robotics.* 2017;33(3):661-674.
28. Liu X, Ge SS, Goh CH, Li Y. Event-triggered coordination for formation tracking control in constrained space with limited communication. *IEEE transactions on cybernetics.* 2018;49(3):1000–1011.
29. Wen G, Chen CP, Liu YJ. Formation control with obstacle avoidance for a class of stochastic multiagent systems. *IEEE Transactions on Industrial Electronics.* 2017;65(7):5847–5855.
30. Yang X, Delin L, Dongyu L, Yancheng Y, Haibin D. Target-enclosing affine formation control of two-layer networked spacecraft with collision avoidance. *Chinese Journal of Aeronautics.* 2019;32(12):2679–2693.
31. Chipade VS, Panagou D. Multiagent planning and control for swarm herding in 2-D obstacle environments under bounded inputs. *IEEE Transactions on Robotics.* 2021;37(6):1956–1972.
32. Chipade VS, Panagou D. Herding an Adversarial Swarm in an Obstacle Environment. In: IEEE 58th Conference on Decision and Control (CDC). 2019:3685-3690.
33. Shen Y, Huang Y. Uniformly observable and globally Lipschitzian nonlinear systems admit global finite-time observers. *IEEE Transactions on Automatic Control.* 2009;54(11):2621–2625.
34. Gajic Z, Qureshi MTJ. *Lyapunov matrix equation in system stability and control*. Courier Corporation, 2008.
35. LaSalle J. Some extensions of Liapunov's second method. *IRE Transactions on circuit theory.* 1960;7(4):520–527.